Comparison of quantum spin Hall states in quasicrystals and crystals

Huaqing Huang[1] and Feng Liu[1,2,*]
[1]*Department of Materials Science and Engineering, University of Utah, Salt Lake City, Utah 84112, USA*
[2]*Collaborative Innovation Center of Quantum Matter, Beijing 100084, China*

(Received 15 April 2019; published 8 August 2019)

We theoretically study the quantum spin Hall states in an Ammann-Beenker-type octagonal quasicrystal and a periodic snub-square crystal, both sharing the same basic building blocks. Although the bulk states show significant differences in localization and transport properties, the topological phases manifest similarly in the two systems. This indicates the robustness of the topological properties regardless of symmetry and periodicity. We characterize the topological nature of the two systems with a nonzero topological invariant (spin Bott index B_s and $\mathbb{Z}_2$ invariant), robust metallic edge states, and quantized conductance. In spite of some quantitative differences, the topological phase diagram of the two systems also exhibits similar behaviors, indicating that the topological phase transition is mainly determined by similar interactions in the two systems regardless of their structural difference. This is also reflected by the observation that the transition point between the normal insulator and the quantum spin Hall state in both systems follows a universal linear scaling relation for topological phase transitions.

DOI: 10.1103/PhysRevB.100.085119

I. INTRODUCTION

Quasicrystals are special states of matter that possess long-range orientational order but no translational symmetry [1]. Without classical crystallographic restriction, quasicrystals may exhibit rotational symmetries that are forbidden in conventional crystals [2]. For example, an eightfold rotational symmetry in octagonal quasicrystals was observed in CrNiSi, VNiSi, and MnSiAl alloys [3–5]. Due to the lack of periodicity, quasicrystals cannot be constructed from a single unit cell as for periodic crystals. However, most quasicrystals can be constructed from two or three types of elementary cells according to certain specified matching rules. For example, the two-dimensional (2D) octagonal quasicrystals are usually described by the Ammann-Beenker tiling with two types of building blocks [6–9], namely squares and 45° rhombi, which can also be used to construct periodic crystals such as the snub-square crystalline lattice [10,11].

On the other hand, quantum spin Hall (QSH) states have been studied in various theoretical models and realistic materials in recent years [12–15]. The QSH state is manifested by an insulating bulk and topologically protected metallic edges with quantized conductance. In general, topological states are insensitive to a smooth modulation of material parameters and cannot change unless the system passes through a topological phase transition (TPT) accompanied by an energy gap closing and reopening process. Such robustness of electronic topology, in principle, guarantees the existence of QSH state in both crystals and quasicrystals regardless of lattice symmetry and periodicity. Previously, we discovered the QSH state in a Penrose-type pentagonal quasicrystal [16,17]. Here, we aim to answer the following question: is there any significant difference of QSH states in quasicrystals versus crystals, especially when they have the same basic building blocks?

To do so, we propose the realization of the QSH state in an octagonal quasicrystal lattice and compare it with the QSH state in a similar crystalline lattice with the same building blocks. The nontrivial electronic topology in the two systems is characterized by the spin Bott index B_s and $\mathbb{Z}_2$ topological invariant, respectively. Due to the bulk-edge correspondence, robust metallic edge states and quantized conductances are observed in both systems. Further analysis of the localization of wave functions indicates that topologically protected metallic edge states in both systems exhibit similar degrees of delocalization, but bulk insulating states in quasicrystals are much more localized than that in crystals, which give rise to a lower bulk conductance. We also mapped out the topological phase diagram for both systems, and we found that the critical points of TPTs in the two systems follow a universal linear scaling relation discovered recently [18].

II. MODEL

The octagonal quasicrystal lattice is constructed according to the Ammann-Beenker tiling [6–9], which includes rhombuses with 45° and 135° angles and squares as basic building blocks [see Fig. 1(a)]. For comparison, we also considered a periodic snub-square crystalline lattice according to the semiregular Archimedean tiling [10,11], as shown in Fig. 1(b). Such a snub-square structure, also known as the snub-quadrille structure, can be constructed by applying a snub operation to a corner-shared square tiling with a rotational angle α. Here we chose $\alpha = 22.5°$ (instead of the conventional $\alpha = 15°$) so that the basic building blocks of both the octagonal quasicrystal and the snub-square crystal are the same, as shown in Fig. 1. We construct real-space

*Author to whom all correspondence should be addressed: fliu@eng.utah.edu

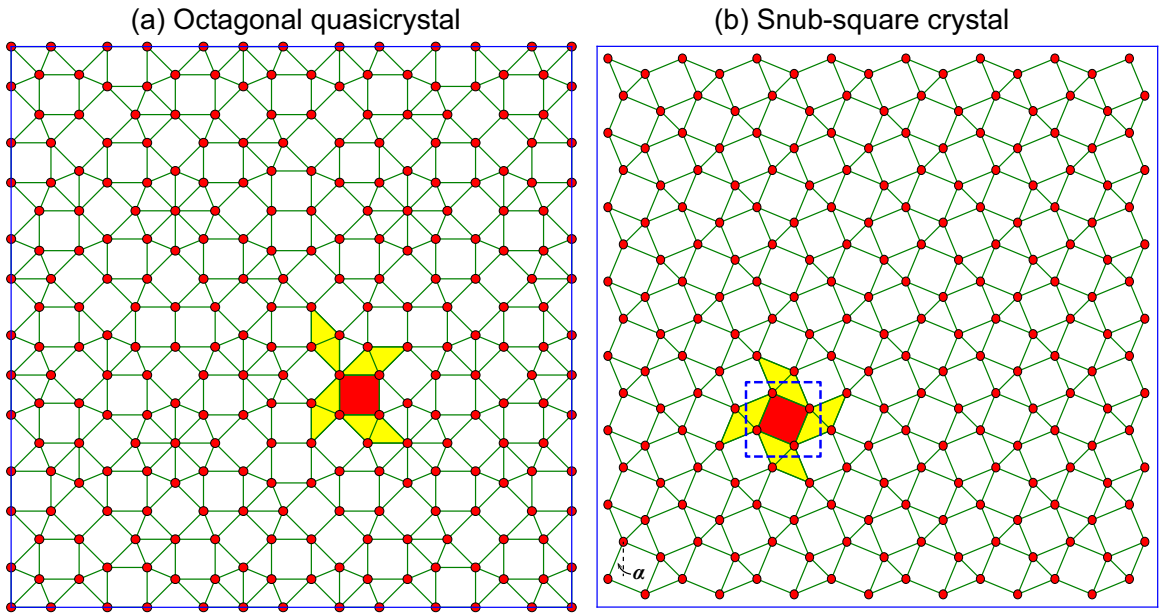

FIG. 1. (a) A periodic approximant of the octagonal quasicrystal lattice obtained from the Ammann-Beenker tiling. (b) A snub-square crystalline lattice based on the semiregular Archimedean tiling. The rotational angle is $\alpha = 22.5^\circ$. The red square and yellow rhombus represent the basic building blocks for both lattices.

tight-binding (TB) models by locating atomic orbitals on the vertices of the tilings. Due to the same building blocks, the first three nearest-neighbor (NN) hoppings in both lattices are the same, which are the short diagonal of the rhombus r_0, the edge of the rhombus or square r_1, and the diagonal of the square r_2, respectively. The proportions of the three distances are $r_0 : r_1 : r_2 = 2\sin\frac{\pi}{8} : 1 : 2\sin\frac{\pi}{4} = \sqrt{2-\sqrt{2}} : 1 : \sqrt{2}$, respectively. For convenience, all the lengths are measured in units of r_1 in our model.

We consider a generic atomic-basis TB model with three orbitals (s, p_x, p_y) per site [16,17,19],

$$H = \sum_{i\alpha} \epsilon_\alpha c^\dagger_{i\alpha} c_{i\alpha} + \sum_{\langle i\alpha, j\beta\rangle} t_{i\alpha,j\beta} c^\dagger_{i\alpha} c_{j\beta} + i\lambda \sum_i \left(c^\dagger_{ip_y} \sigma_z c_{ip_x} - c^\dagger_{ip_x} \sigma_z c_{ip_y} \right), \quad (1)$$

where $c^\dagger_{i\alpha} = (c^\dagger_{i\alpha\uparrow}, c^\dagger_{i\alpha\downarrow})$ are electron creation operators on the $\alpha(= s, p_x, p_y)$ orbital at the ith site. ϵ_α is the on-site energy of the α orbital. $t_{i\alpha,j\beta} = t_{\alpha\beta}(\mathbf{r}_{ij})$ is the hopping integral between α and β orbitals at the ith and jth sites, respectively. λ is the spin-orbit coupling (SOC) strength and σ_z is the Pauli matrix. The hopping integral follows the Slater-Koster (SK) parametrization [20],

$$t_{\alpha\beta}(\mathbf{r}_{ij}) = \mathrm{SK}[\mathbb{V}_{\alpha\beta\delta}(r_{ij}), \hat{\mathbf{r}}_{ij}], \quad (2)$$

where $\hat{\mathbf{r}}_{ij}$ is the unit direction vector. The distance dependence of the bonding parameters $\mathbb{V}_{\alpha\beta\delta}(r_{ij})$ ($\delta = \sigma$ or π) is captured approximately by the Harrison relation [21],

$$\mathbb{V}_{\alpha\beta\delta}(r_{ij}) = V_{\alpha\beta\delta} \frac{\gamma^2}{r_{ij}^2}, \quad (3)$$

where $V_{\alpha\beta\delta}$ is a constant [22–24] and γ is a scaling factor to uniformly tune the bonding strengths [25,26]. Since only the band inversion between s and p states of different parities is important for the realization of topological states, we focus only on 2/3 filling of electron states hereafter.

III. STRUCTURAL SIMILARITY AND DIFFERENCE

We first compared the structures of the two lattices. Although the first three NN distances in the two lattices are the same due to the same basic building blocks, the corresponding coordination numbers are different. For the snub-square crystalline lattice, the coordination numbers are $z_0 : z_1 : z_2 = 1 : 4 : 2$, which can be easily counted from its periodic unit cell. However, for the octagonal quasicrystal lattice, we cannot directly obtain the coordination number due to its quasiperiodicity. Instead, we generated a large patch of the underlying pattern of the octagonal quasicrystal, which contains more than 8119 atoms, and we calculated the coordination numbers as $z_0 : z_1 : z_2 \approx 1.172 : 4 : 2.485$. Such a structural difference between the octagonal quasicrystal and the snub-square crystal gives rise to a quantitative difference in electronic structures, as discussed later.

IV. ENERGY SPECTRUM AND REAL-SPACE EDGE STATES

Subsequently, we studied the energy spectrum of the octagonal quasicrystal and the snub-square crystal, respectively. The results of an octagonal quasicrystal lattice containing 1393 atoms with a periodic boundary condition (PBC) and an open boundary condition (OBC) are shown in Fig. 2(a). In the presence of a PBC, the system shows an energy gap, indicating that the system is an insulator. However, there are some eigenvalues within the gap in the presence of an OBC, implying that the OBC system becomes metallic. We found that the typical midgap states mainly distribute at the

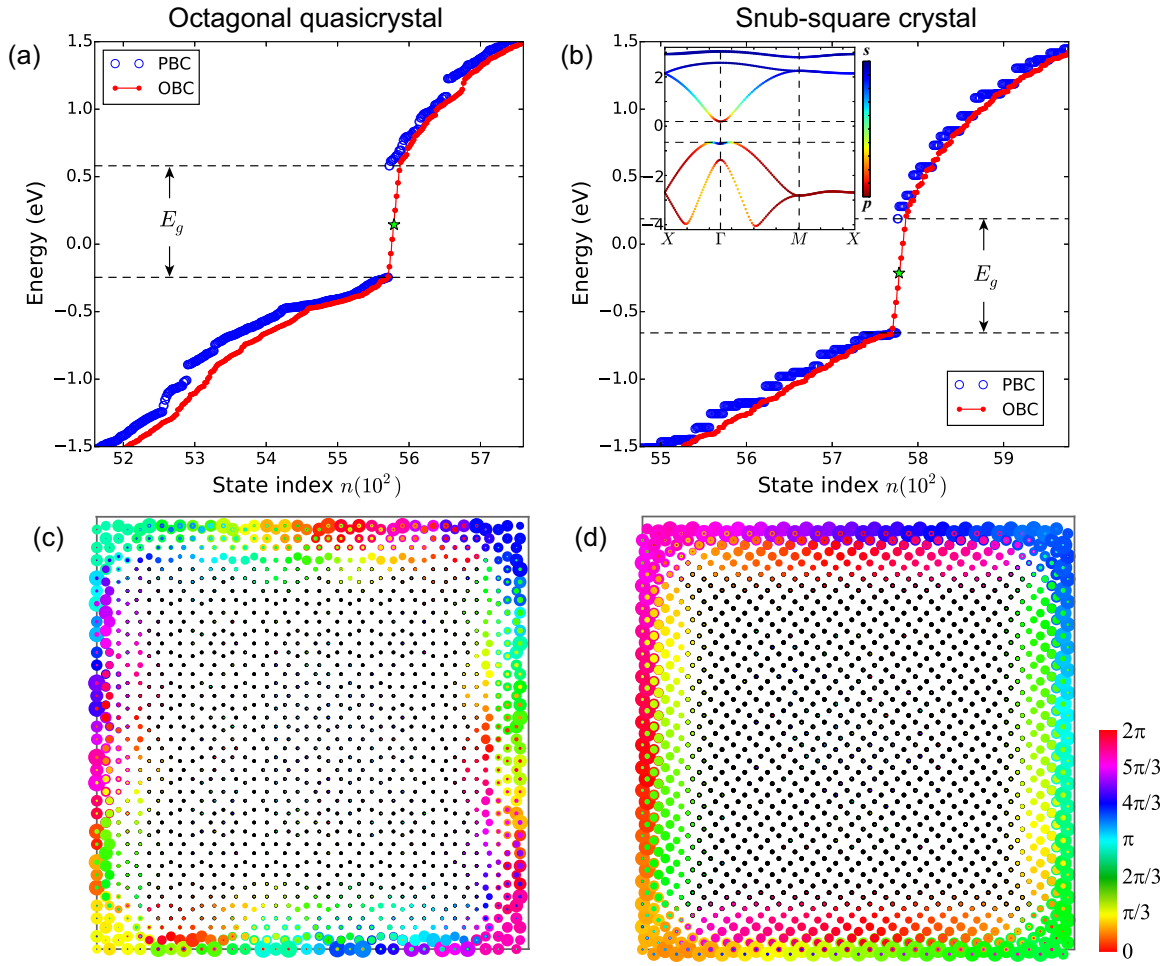

FIG. 2. Calculation of (a,c) an Ammann-Beenker-type octagonal quasicrystal lattice with 1393 atoms and (b,d) a 19 × 19 snub-square crystalline lattice with 1444 atoms (three orbitals and two spins on each atom). The parameters used here are $\epsilon_s = 1.8$, $\epsilon_p = -6.5$, $\lambda = 0.8$, $V_{ss\sigma} = -0.4$, $V_{sp\sigma} = 0.9$, $V_{pp\sigma} = 1.8$, $V_{pp\pi} = 0.05$ eV, and $\gamma = 0.97$. (a,b) Energy eigenvalues E_n vs the state index n. The inset of (b) shows the band structure of the snub-square crystal. (c,d) The wave function $|\psi(\mathbf{r})\rangle = \chi(\mathbf{r})e^{i\phi(\mathbf{r})}$ of the midgap state [marked as the green star in (a) and (b)] is distributed on the edge of the system. The size and the color of the blobs indicate the norm $|\chi(\mathbf{r})|^2$ and phase $\phi(\mathbf{r})$ of the wave function, respectively.

boundary of the finite sample, as shown in Fig. 2(c). Moreover, the study of other samples with different boundary geometries indicates that these "edge states" always remain on the boundaries (see the Supplemental Material [27]). Apparently, these delocalized "edge states" within the energy gap are different from typical bulk states, which exhibit localized or critical characters of quasicrystals. Due to the time-reversal symmetry, the midgap states always appear in pairs with the same energy but opposite spin polarizations. Next, for a direct comparison, we calculated the energy spectrum of a 19 × 19 supercell of the snub-square crystal, which is of similar size to the octagonal quasicrystal sample discussed above. Similarly, the PBC system of the snub-square crystal clearly shows an energy gap, while the OBC system exhibits midgap states, as shown in Fig. 2(b). The real-space distribution of these midgap states also shows metallic edge-state characteristics, which are located on the boundary of the OBC sample [see Fig. 2(d)]. The comparable electronic structures of the octagonal quasicrystal and the snub-square crystal imply similar topological states in the two systems.

V. TOPOLOGICAL INVARIANTS

To further confirm the electronic topology in the two lattices, we calculate the $\mathbb{Z}_2$ topological invariant [28] for the snub-square crystal and the spin Bott index B_s, which is a newly defined topological invariant for QSH states in nonperiodic systems [16,17], for the octagonal quasicrystal, respectively. The spin Bott index $B_s = \frac{1}{2}(B_+ - B_-)$ is defined as the half-difference between the Bott indices for the spin-up and spin-down sectors: $B_\pm = \frac{1}{2\pi}\mathrm{Im}\{\mathrm{tr}[\ln(V_\pm U_\pm V_\pm^\dagger U_\pm^\dagger)]\}$, where $U_\pm = P_\pm e^{i2\pi X} P_\pm + (I - P_\pm)$ and $V_\pm = P_\pm e^{i2\pi Y} P_\pm + (I - P_\pm)$ are the projected position operators, with $P_\pm$ being the projectors onto the occupied states and $\{X, Y\}$ are the normalized coordinates defined between [0,1) [16,17]. The calculated $\mathbb{Z}_2 = 1$ and spin Bott index $B_s = 1$ indicate that the two systems are QSH insulators. The nontrivial topological states are attributed to the band inversion between the s-dominated conduction state and the p-dominated valence states. Based on a primitive-cell calculation, we obtained the band structure of the snub-square crystal along high-symmetry paths of the

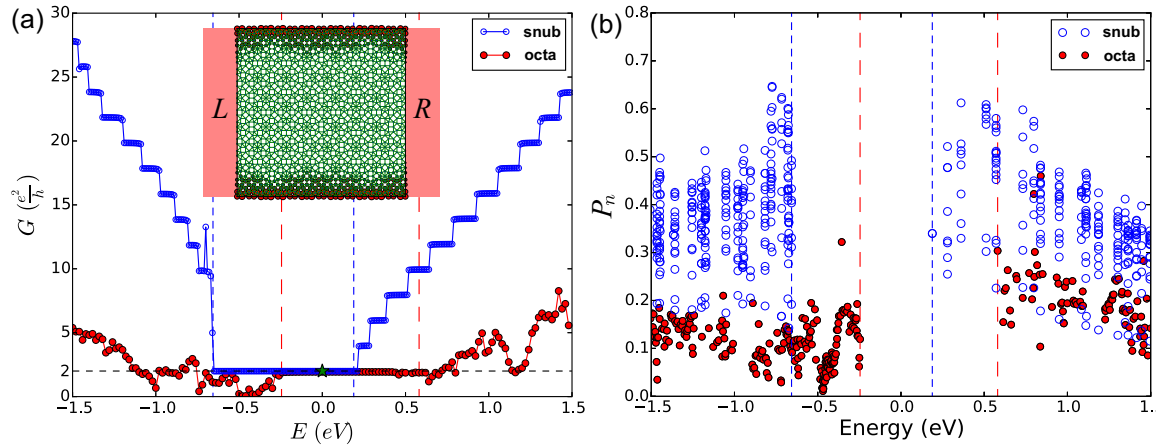

FIG. 3. Transport simulation of an octagonal quasicrystal and a snub-square crystal. (a) Two-terminal conductance G as a function of the Fermi energy E showing a quantized plateau in the energy gap. The inset shows the local density of states $\rho_i(E)$ at $E = 0$ eV [marked as the green star in (a)] for the central part of the octagonal quasicrystal in the transport simulation, where the size of the red dot represents the relative value of $\rho_i(E)$. (b) Participation ratio P_n of an octagonal quasicrystal and a snub-square crystal with PBCs. The blue and red dashed lines mark the gap for the octagonal quasicrystal and the snub-square crystal, respectively.

Brillouin zone. As show in the inset of Fig. 2(b), a band inversion occurs around the Γ point. Similar band inversions also appear in the orbital-solved spectrum of the octagonal quasicrystal [27]. According to the bulk-edge correspondence, it is natural to expect the existence of metallic edge states for both systems. Therefore, the nontrivial topological invariants are consistent with the presence of bulk gap and robust edge states, unambiguously identifying the nontrivial topological nature of the octagonal quasicrystal and the snub-square crystal.

VI. TRANSPORT PROPERTIES

To verify the metallic feature of the edge states, we studied the transport properties of the two systems based on the nonequilibrium Green's function method [29–31]. As shown in Fig. 3(a), the two-terminal charge conductance shows a clear quantized plateau at $G = 2e^2/h$ within the gap region for both the octagonal quasicrystal and the snub-square crystal, which resembles that of the QSH state in a graphene lattice as predicted by Kane and Mele [32]. Remarkably, the local density of state of the central quasicrystal at $E = 0$ eV [see the inset of Fig. 3(a)] is mainly distributed on two open side edges of the quasicrystal, indicating that the conductive channels are mainly contributed by the topologically protected edge states. It is worth noting that there are also quantized plateaus outside the gap (in the bulk region) for the snub-square crystal. This is because the same periodic snub-square crystal is used for the left and right leads and the central part in the transport simulation (see the Supplemental Material [27]). Due to the periodic structure of the transport simulation setup, no scatting occurs within the ballistic transport approximation. Hence, the quantized conductance actually provides the upper bound of the conductance at the ideal situation without any scatterings. Such quantized plateaus, which are different from the topologically protected quantized conductance within the gap region, can be destroyed by impurity, vacancy scattering, or contact resistance, thus they are not robust.

Another important point is that the conductance of the octagonal quasicrystal is much smaller than that of the periodic snub-square crystal outside the gap region. This actually indicates that the octagonal quasicrystal is a weak metal compared with the snub-square crystal. The low conductance of quasicrystals is also consistent with previous studies [33,34]. Generally speaking, the transport properties are dramatically affected by the localization of the wave functions. Due to the critical behavior (power-law decay) of bulk wave functions in quasicrystals [35–38], it is expected that the weak-metallic characteristic is a quite universal property of quasicrystals.

VII. LOCALIZATION OF WAVE FUNCTIONS

To compare the localization of wave functions in the octagonal quasicrystal and the snub-square crystal, we calculate the participation ratio P_n of each state in both systems. The participation ratio is given by [39]

$$P_n = \frac{\left(\sum_i^N |\langle i|\psi_n\rangle|^2\right)^2}{N\sum_i^N |\langle i|\psi_n\rangle|^4}, \tag{4}$$

where $|i\rangle$ is the ith local orbital basis. As shown in Fig. 3(b), the participation ratio P_n of most wave functions in the octagonal quasicrystal is much smaller than that of the Bloch states in the snub-square crystal. This is because the Bloch states in periodic lattices are modulated plane waves that are extended throughout the whole system, while the critical states in quasicrystals are generically found to be localized with algebraic spatial decay [40–42]. The significant difference in the participation ratio P_n is also consistent with the weak-metallic behavior of the octagonal quasicrystal in the electronic transport discussed above. Interestingly, the participation ratios of the topological edge states in both systems are very close, which is roughly proportional to the perimeter/area ratio of the sample [see Figs. 2(c) and 2(d)] [27]. Due to the 1D feature of the edge states, we further calculated the Thouless exponent (Lyapunov coefficient) $l(E_i)$

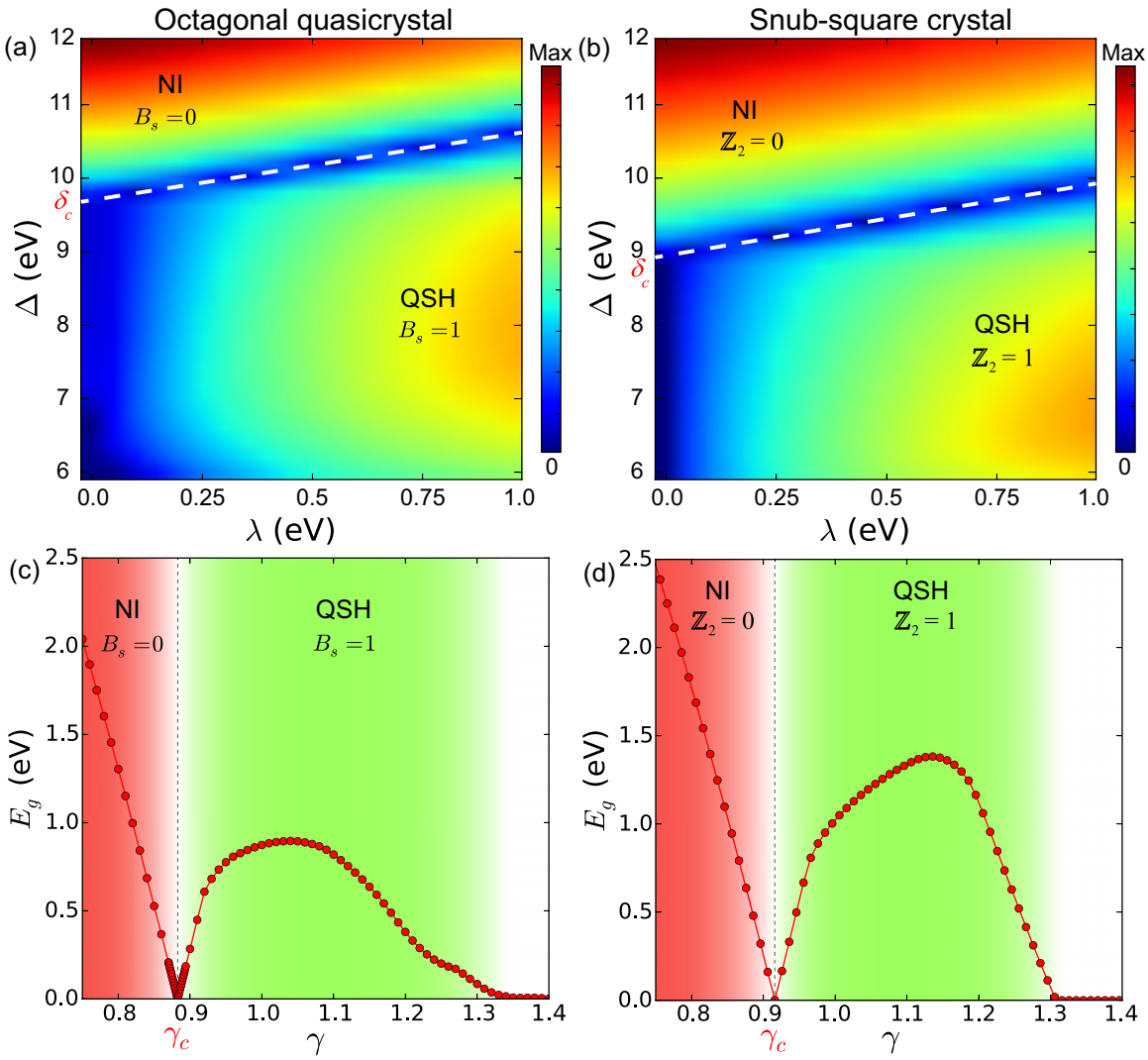

FIG. 4. (a,b) Topological phase diagram for (a) the octagonal quasicrystal and (b) the snub-square crystal in the parameter space of energy difference $\Delta = \epsilon_s - \epsilon_p$ and SOC strength λ. The color represents the size of the bulk energy gap. (c,d) Energy gap E_g and topological invariant ($\mathbb{Z}_2$ invariant or spin Bott index B_s) as a function of bonding strength scale γ for (c) the octagonal quasicrystal and (d) the snub-square crystal. A TPT between a normal insulator (NI) and a QSH insulator is clearly visible.

[43–47] for edge states in both systems,

$$l(E_i) = \int dE' \rho(E') \ln |E' - E_i| = \frac{1}{N-1} \sum_{j \neq i} \ln |E_j - E_i|, \tag{5}$$

where $\rho(E')$ is the density of states. The Thouless exponent $l(E)$ is proportional to the inverse of the localization length of states in 1D systems, i.e., $l(E) \sim 1/\xi$. The calculated $l(E_i)$ are almost the same for the topological edge states in the two lattices, indicating a similar decay length of topological edge states in both systems. Therefore, QSH states in quasicrystals and crystals manifest similarly, even though their bulk states are significantly different.

VIII. TOPOLOGICAL PHASE DIAGRAM

One of the essential conditions to achieve the QSH state is the band inversion between conduction and valence states, which enables the TPT between a normal insulator (NI) and a QSH insulator. Typically, one can realize the band inversion by tuning the on-site energy difference $\Delta = \epsilon_s - \epsilon_p$, the SOC strength λ, and the bonding strength γ [14,15]. According to the universal linear scaling of TPT we derived recently [18], the critical transition point is roughly determined by the condition

$$\Delta - \lambda \propto \left(\frac{\gamma}{L}\right)^2. \tag{6}$$

Here L is the average bond length of a given lattice, defined as

$$\frac{1}{L^2} = \frac{1}{2} \sum_i \frac{z_i}{r_i^2}, \tag{7}$$

where the summation runs over all the bonds within the cutoff r_{cut}. Based on the coordination number z_i and bond length r_i listed above, one can easily obtain $L^{\text{octa}} = 0.525$ and $L^{\text{snub}} = 0.546$ (in units of r_1) for the octagonal quasicrystal and the snub-square crystal, respectively. The topological phase

diagrams of the two lattices should be related to each other according to the relation Eq. (6).

We studied the topological phase diagram in the Δ-λ plane at a fixed γ for both lattices. As shown in Figs. 4(a) and 4(b), the NI and QSH states are separated by a line of zero-energy gap in both systems. By tracing the evolution of topological invariants for the two systems, it is found that there is a sharp jump in the topological invariant across the phase boundary, indicating the occurrence of a TPT. Interestingly, the linear lines of the energy gap closing in the two systems exhibit a similar slope but different intercepts,

$$\Delta = \lambda + \delta_c. \tag{8}$$

Such a linear behavior agrees with the critical condition Eq. (6) with given γ and L in the two systems, respectively. Moreover, according to the critical condition, the intercepts δ_c of the two lattices are related by

$$\frac{\delta_c^{\text{octa}}}{\delta_c^{\text{snub}}} = \left(\frac{L^{\text{snub}}}{L^{\text{octa}}}\right)^2. \tag{9}$$

Based on the numerical calculations, we obtained $\delta_c^{\text{octa}} \approx 9.67$ eV and $\delta_c^{\text{snub}} \approx 8.93$ eV, which satisfy the relation in Eq. (9).

Furthermore, we investigated the phase evolution with the increasing bonding strength γ at given Δ and λ. As shown in Figs. 4(c) and 4(d), the energy gap decreases to zero and reopens with increasing γ in both systems, which is associated with a TPT from a NI to a QSH state. Apparently, a band inversion occurs at the critical transition point where $\gamma_c^{\text{octa}} = 0.883$ and $\gamma_c^{\text{snub}} = 0.916$ (in unit of r_1) for the two systems, respectively. According to the critical condition (6), it is straightforward to find that these critical values obey the following relation:

$$\frac{\gamma_c^{\text{snub}}}{\gamma_c^{\text{octa}}} = \frac{L^{\text{snub}}}{L^{\text{octa}}}. \tag{10}$$

Therefore, although the two systems show some quantitative difference in the TPT due to the structural difference, they are, in fact, related by a simple critical condition (6). The above connection of TPTs in between quasicrystals and crystals is not only valid for the two specific cases in this work, but it is expected to be a general phenomenon for other quasicrystalline, crystalline, and even disordered systems [18]. Generally, the QSH state can appear in quasicrystals of different local isomorphism (LI) classes, however the critical point of TPT varies with the LI classes. Because different LI classes have the same symmetry and fundamental repeating units but different space-filling arrangements of repeating units [48], the local distribution of vertex environment and hence the average bond length varies with LI classes [49].

IX. CONCLUSION

We have proposed the realization of the QSH state in an Ammann-Beenker-type octagonal quasicrystal and compared it with the QSH state in a periodic snub-square crystal. Although the two systems are different in symmetry and periodicity, they share the same building blocks. Based on a generic TB model, we discover that even though the bulk wave functions of the two systems are significantly different, the existence of topological states is robust regardless of symmetry and periodicity. The topological manifestations of QSH states, such as robust edge states, topological invariant, and quantized conductance in the quasicrystal and crystal, are very similar. We also compared the topological phase diagrams of the two systems and found that the critical points of TPTs in both systems can be described by a universal relation. Our findings not only provide a better understanding of the compatibility of general critical states in quasicrystals with extended topological states, but also significantly ease the practical fabrication of topological materials without a stringent requirement for structural control.

ACKNOWLEDGMENTS

This work was supported by U.S. DOE-BES (Grant No. DE-FG02-04ER46148). The calculations were done on the CHPC at the University of Utah and U.S. the National Energy Research Scientific Computing Center (NERSC) at the Office of Science in the U.S. Department of Energy.

[1] D. Shechtman, I. Blech, D. Gratias, and J. W. Cahn, Phys. Rev. Lett. **53**, 1951 (1984).
[2] D. Levine and P. J. Steinhardt, Phys. Rev. Lett. **53**, 2477 (1984).
[3] N. Wang, H. Chen, and K. H. Kuo, Phys. Rev. Lett. **59**, 1010 (1987).
[4] J. C. Jiang, N. Wang, K. K. Fung, and K. H. Kuo, Phys. Rev. Lett. **67**, 1302 (1991).
[5] N. Wang, K. K. Fung, and K. Kuo, Appl. Phys. Lett. **52**, 2120 (1988).
[6] B. Grünbaum and G. C. Shephard, *Tilings and Patterns* (W. H. Freeman and Company, New York, 1987).
[7] F. P. M. Beenker, *Algebraic Theory of Non-periodic Tilings of the Plane by Two Simple Building Blocks: A Square and a Rhombus* (Eindhoven University of Technology, Eindhoven, The Netherlands, 1982).
[8] M. Duneau, R. Mosseri, and O. Christophe, J. Phys. A **22**, 4549 (1989).
[9] P. Kramer and Z. Papadopolos, *Coverings of Discrete Quasiperiodic Sets: Theory and Applications to Quasicrystals* (Springer-Verlag Berlin Heidelberg, 2003), Vol. 180.
[10] D. Chavey, Comput. Math. Appl. **17**, 147 (1989).
[11] S. Walter and S. Deloudi, *Crystallography of Quasicrystals: Concepts, Methods and Structures* (Springer-Verlag Berlin Heidelberg, 2009), Vol. 126.
[12] M. Z. Hasan and C. L. Kane, Rev. Mod. Phys. **82**, 3045 (2010).
[13] X.-L. Qi and S.-C. Zhang, Rev. Mod. Phys. **83**, 1057 (2011).
[14] H. Huang, Y. Xu, J. Wang, and W. Duan, WIRES: Comp. Mol. Sci. **7**, e1296 (2017).
[15] Z. Wang, K.-H. Jin, and F. Liu, WIRES: Comp. Mol. Sci. **7**, e1304 (2017).
[16] H. Huang and F. Liu, Phys. Rev. Lett. **121**, 126401 (2018).
[17] H. Huang and F. Liu, Phys. Rev. B **98**, 125130 (2018).
[18] H. Huang and F. Liu, arXiv:1904.06003.
[19] Z. Wang, K.-H. Jin, and F. Liu, Nat. Commun. **7**, 12746 (2016).

[20] J. C. Slater and G. F. Koster, Phys. Rev. **94**, 1498 (1954).
[21] W. A. Harrison, *Electronic Structure and the Properties of Solids: The Physics of the Chemical Bond* (Courier Corporation, North Chelmsford, MA, 2012).
[22] W. A. Harrison, Phys. Rev. B **24**, 5835 (1981).
[23] M. van Schilfgaarde and W. A. Harrison, Phys. Rev. B **33**, 2653 (1986).
[24] M. Kitamura and W. A. Harrison, Phys. Rev. B **44**, 7941 (1991).
[25] G. Grosso and C. Piermarocchi, Phys. Rev. B **51**, 16772 (1995).
[26] L. Shi and D. A. Papaconstantopoulos, Phys. Rev. B **70**, 205101 (2004).
[27] See Supplemental Material at http://link.aps.org/supplemental/10.1103/PhysRevB.100.085119 for more details about the calculated results.
[28] A. A. Soluyanov and D. Vanderbilt, Phys. Rev. B **83**, 235401 (2011).
[29] S. Datta, *Electronic Transport in Mesoscopic Systems* (Cambridge University Press, Cambridge, 1997).
[30] M. Büttiker, Phys. Rev. B **38**, 9375 (1988).
[31] H. Huang, Z. Wang, N. Luo, Z. Liu, R. Lü, J. Wu, and W. Duan, Phys. Rev. B **92**, 075138 (2015).
[32] C. L. Kane and E. J. Mele, Phys. Rev. Lett. **95**, 226801 (2005).
[33] E. S. Zijlstra, Phys. Rev. B **66**, 214202 (2002).
[34] B. Passaro, C. Sire, and V. G. Benza, Phys. Rev. B **46**, 13751 (1992).
[35] M. Kohmoto, B. Sutherland, and C. Tang, Phys. Rev. B **35**, 1020 (1987).
[36] H. Tsunetsugu, T. Fujiwara, K. Ueda, and T. Tokihiro, J. Phys. Soc. Jpn. **55**, 1420 (1986).
[37] T. Janssen, *The Mathematics of Long-Range Aperiodic Order* (Kluwer, Dordrecht, The Netherlands, 1997).
[38] Z. M. Stadnik, *Physical Properties of Quasicrystals* (Springer-Verlag Berlin Heidelberg, 1999), Vol. 126.
[39] T. Odagaki and D. Nguyen, Phys. Rev. B **33**, 2184 (1986).
[40] C. Sire, Europhys. Lett. **10**, 483 (1989).
[41] V. G. Benza and C. Sire, Phys. Rev. B **44**, 10343 (1991).
[42] Y. Zhang and X. Fu, Solid State Commun. **149**, 605 (2009).
[43] D. Thouless, J. Phys. C **5**, 77 (1972).
[44] D. J. Thouless, Phys. Rev. Lett. **39**, 1167 (1977).
[45] S. Das Sarma, S. He, and X. C. Xie, Phys. Rev. Lett. **61**, 2144 (1988).
[46] H. Cruz and S. D. Sarma, J. Phys. I **3**, 1515 (1993).
[47] P. Tong, B. Li, and B. Hu, Phys. Rev. Lett. **88**, 046804 (2002).
[48] R. Ingalls, J. Non-Cryst. Solids **153-154**, 177 (1993).
[49] C. Lin, P. Steinhardt, and S. Torquato, J. Phys.: Condens. Matter **29**, 204003 (2017).